Porphyrin and Ligand Protons as Internal Labels for Determination of Ligand Orientation in ESEEMS of Low-Spin d^5 Complexes in Glassy Media: ESEEM Studies of the Orientation of the **g** Tensor with Respect to the Planes of Axial Ligands and Porphyrin Nitrogens of Low-Spin Ferriheme Systems

Arnold M. Raitsimring* and F. Ann Walker*

Contribution from the Department of Chemistry, University of Arizona, Tucson, Arizona 85721

Received July 8, 1997. Revised Manuscript Received October 24, 1997

Abstract: The proton sum frequency peak(s), $I(\nu_+)$, in the ESEEM spectra of low-spin ferriheme complexes provide single-crystal-like information concerning the orientation of the **g** tensor in samples in frozen glassy media. In this work we have investigated two model heme complexes, $[OEPFe(imidazole)_2]^+$ and $[OEPFe(4\text{-(dimethylamino)pyridine})_2]^+$ (OEP = octaethylporphyrinate). Both experimental intensities and frequency shifts from twice the ^1H Larmor frequency of the observed signals were measured at various points across the EPR spectrum and compared to the expected spectra, simulated using the known crystal structure data, isotropic hyperfine coupling constants, and *g* strain. In each case the *z* magnetic axis direction was defined as perpendicular to the mean plane of the porphyrinate, and it was found that g_{zz} is the largest *g* value in both cases. The in-plane magnetic axis directions could also be determined from the ESEEM data, and it was found that the orientations of g_{xx} and g_{yy} differ, depending on the orientation of the (parallel) axial ligands with respect to the porphyrinate nitrogens: For the bis(imidazole) complex, for which the axial ligands nearly eclipse opposite porphyrinate nitrogens ($\phi = 7°$) in the crystalline state, g_{xx} and g_{yy} are aligned at ±45° to the normal to the plane of the axial ligands, while for the bis(4-(dimethylamino)pyridine) complex, for which the axial ligands lie in parallel planes nearly bisecting the porphyrinate nitrogens ($\phi = 41°$) in the crystalline state, g_{yy} is aligned along the plane of the axial ligands. The significance of these results with respect to the concept of counterrotation of the **g** tensor with rotation of axial ligands and the interpretation of the in-plane magnetic anisotropy of heme proteins measured by NMR techniques is discussed.

Introduction

Low-frequency nuclei such as ^{14}N, ^{15}N, and ^2H have traditionally been used as probes of the magnetic environment of the ferriheme and substituted metalloporphyrin centers of heme proteins in ESEEM spectroscopy.[1−5] However, the signals from quadrupolar nuclei are difficult to deconvolute without the combination of isotopic labeling and extensive spectral simulation, and, even if deconvolution is successful, little information is usually obtained concerning the *orientation* of the **g** tensor with respect to the porphyrin nitrogens and the axial ligands. To our knowledge there is only one example of ENDOR experiments where the metal−nitrogen interaction was used for determination of the ordering of *g* values.[6] However, in this case the information was obtained from the hyperfine, not the quadrupole interaction.[6] In contrast, Dikanov,[7] McCracken,[8] and we[9] have each shown recently that the proton sum frequency peak(s), $I(\nu_+)$, can provide single-crystal-like information concerning the orientation of the **g** tensor from samples in frozen glassy media. We recently investigated a model ferriheme complex, $[TPPFe(pyrazole)_2]^+$, [9] and showed that because of the angle selection of the ESEEM experiment, it was possible to determine unambiguously that g_{zz}, the *g* value aligned along the molecular *z* axis and perpendicular to the mean plane of the porphyrin, is the largest *g* value for this complex, even though the crystal field parameters, the rhombicity (V/Δ) and Tetragonality (Δ/λ),[10] calculated from this assignment "violate" the conditions of Taylor's "Proper Axis System," i.e., that $V/\Delta \leq {}^2/_3$.[11] This finding resulted from a careful investigation of the magnetic field dependence of the intensity of the "distant proton" (DP) signal at twice the proton Larmor frequency.[9]

The nearest protons (NP) to the low-spin Fe(III) center, the α-H of the pyrazole ligands, which are at 3.1−3.2 Å from the metal, provided the information concerning the orientation of

(1) Mims, W. B.; Peisach, J. *J. Chem. Phys.* **1978**, *69*, 4921.
(2) Magliozzo, R. S.; Peisach, J. *Biochemistry* **1992**, *31*, 189.
(3) Lee, H. C.; Ikeda-Saito, M.; Yonetani, T.; Magliozzo, R. S.; Peisach, J. *Biochemistry* **1992**, *31*, 7274.
(4) Magliozzo, R. S.; Peisach, J. *Biochemistry* **1993**, *32*, 8446.
(5) Lee, H. C.; Peisach, J.; Tsuneshige, A.; Yonetani, T. *Biochemistry* **1995**, *34*, 6883.
(6) Doan, P. E.; LaChance-Galang, K.; Clarke, M. J. Manuscript in preparation.
(7) (a) Tyrishkin, A. M.; Dikanov, S. A.; Evelo, R. G.; Hoff, A. J. *J. Chem. Phys.* **1992**, *97*, 42. (b) Tyrishkin, A. M.; Dikanov, S. A.; Goldfarb, D. *J. Magn. Reson.* **1993**, *A105*, 271.
(8) (a) McCracken, J.; Freidenberg, S. *J. Phys. Chem.* **1994**, *98*, 467. (b) Lee, H.; McCracken, J. *J. Phys. Chem.* **1994**, *98*, 12861.
(9) Raitsimring, A. M.; Borbat, P.; Shokhireva, T. Kh.; Walker, F. A. *J. Phys. Chem.* **1996**, *100*, 5235.
(10) (a) Blumberg, W. E.; Peisach, J. In *Structure and Bonding of Macromolecules and Membranes*; Chance, B., Yonetani, T., Eds.; Academic: New York, 1971; p 215. (b) Peisach, J.; Blumberg, W. E.; Adler, A. D. *Ann. N. Y. Acad. Sci.* **1973**, *206*, 310.
(11) Taylor, C. P. S. *Biochim. Biophys. Acta* **1977**, *491*, 137.

S0002-7863(97)02264-6 CCC: $15.00
Published on Web 01/22/1998

g_{xx}: The magnetic field dependence of the intensity of the NP doublet signal was shown to be consistent with the minimum g value, g_{xx} being aligned *along* the direction of the α-H of the pyrazole ligands, or, that is, g_{xx} lies along the nodal plane of the (as we had assumed, coparallel) pyrazoles.[9] Although the crystal structure of this complex has been completed,[12] we suspected that the axial ligand dihedral angles of 45° and 54° found for the two independent molecules in the unit cell may not represent the structure of the complex in frozen, glassy solutions, and thus we were left with no clear proof as to how the orientation of the in-plane **g** tensor related to the nitrogens of the porphyrin ring. We pointed out at that time that if g_{xx} is oriented along the plane of the axial ligands, then g_{yy} is oriented along the direction of the filled p_π orbital of the axial ligands, and that this has been shown to be the case for several model heme complexes[13] and several heme proteins, including cytochrome *c*[14] (where one of the p_π orbitals in question is that of the methionine sulfur, and the histidine and methionine ligands appear to contribute essentially equally[15]), sperm whale cyanometmyoglobin,[16,17] and the cyanide complex of horseradish peroxidase.[18] However, for other ferriheme model compounds[19] and proteins, most notably ferricytochrome b_5,[17,20,21,22] the **g** tensor has been found to be rotated by about 90°, such that g_{yy} is oriented close to the nodal plane of the axial ligands and g_{xx} is along the direction of the p_π orbital of those ligands. On the basis of the work reported herein, we can now explain these seemingly contradictory findings as being due to the counterrotation of the **g** tensor with rotation of the axial ligands from the N_P-Fe-N_P axis to an angle of approximately 45°, to lie along opposite *meso* positions of the porphyrin, the bisector of the Fe−N bonds. This concept of counterrotation was first mentioned by Oosterhuis and Lang,[23] with respect to the relative orientation of the **g** and hyperfine tensors in a system that had no planar ligands, and then shown by Strouse and co-workers[19] to occur in model heme complexes in which the axial ligand planes lay along the *meso* positions of the porphyrin ring. However, it has not been widely accepted or understood, although it has recently been assumed to occur, and has been used as such to calculate the dipolar (pseudocontact) contributions to the NMR shifts of ferricytochrome *c*.[15]

In this work ESEEM spectroscopy has been used to define the orientation of the **g** tensor in two octaethylporphyrinatoiron-(III) bis-ligand complexes, structure I, for which crystal

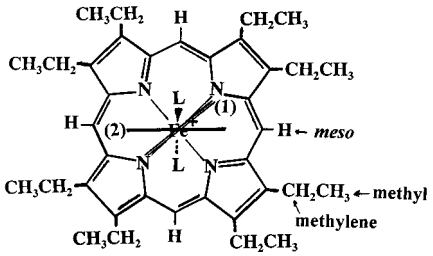

L = d_4- or h_4-Imidazole (1)
L = 4-Dimethylaminopyridine (2)

structures are available: For the case of L = 4-(dimethylamino)-pyridine, the angle that describes the rotation of the projection of the ligand planes from the N_P-Fe-N_P axis, $\phi = 41°$,[24] and thus the ligands lie very close to the *meso* positions of the porphyrin, and for the case of L = imidazole, where $\phi = 7°$ in the solid state.[25] As will be shown, g_{yy} is aligned along the nodal plane of the 4-NMe_2Py ligands (90° different than in $[TPPFe(PzH)_2]^+$ [9]), while g_{xx} and g_{yy} are aligned at angles of ±45° to the normal of the plane of the imidazole ligands. In distinction to the previous study,[9] for the 4-(dimethylamino)-pyridine complex *all* information concerning the orientation of the **g** tensor (both g_{zz} and g_{xx}) has been obtained from the NP peak(s). In the companion work,[26] we have explored the theoretical basis for the counterrotation of the **g** tensor with axial ligand rotation and have shown that the angular dependence may not be simply linear and that corotation can be observed in some cases.

Experimental Section

Samples of the bis(imidazole-h_4 and -d_4)octaethylporphyrinatoiron-(III), $[OEPFe(h_4-Im)_2]^+Cl^-$ and $[OEPFe(d_4-Im)_2]^+Cl^-$, were prepared from OEPFeCl synthesized in this laboratory and a fresh sample of imidazole (Aldrich) or d_4-imidazole (Cambridge Isotopes), respectively, by dissolving a 1:3 molar ratio of the two reactants in deuterated dimethylformamide−acetonitrile (Cambridge Isotopes) in a 1:3 ratio. Samples of the bis(4-(dimethylamino)pyridine)octaethylporphyrinatoiron-(III), $[OEPFe(4\text{-}NMe_2Py)_2]^+Cl^-$, were prepared from OEPFeCl and a fresh sample of 4-NMe_2Py (Aldrich) by dissolving a 1:3 molar ratio of the two compounds in deuterated dichloromethane (Cambridge Isotopes) or CD_2Cl_2−toluene-d_8 (Cambridge Isotopes) mixtures in the ratios 1:1, 1:2, and 1:5. For the latter complex, the cw EPR spectra were investigated to determine which gave the sharpest, best resolved rhombic spectrum. It was found that the 1:2 mixed-solvent ratio produced the best spectral qualities, and thus this mixture was used for all ESEEM spectra. The concentrations of the complexes used for ESE measurements was ~1 mM. Such samples yield a rather large initial ESE signal at dead time pulse separation over the entire field range over which measurements were performed. To avoid amplifier saturation the initial signal was attenuated by 15−20 db.

Continuous wave EPR spectra were obtained on a Bruker ESP-300E spectrometer operating at X-band. A Systron-Donner microwave counter was used for measuring the frequency. The EPR measurements were performed at 4.2 K using an Oxford continuous flow cryostat, ESR 900. Pulsed EPR studies were performed on a home-built spectrometer that has been described previously.[27] ESEEM measurements were done at the operational mw frequencies $\nu_0 = 8.702-8.804$ GHz, using a reflecting cavity which mates with the Oxford cryostat. Two microwave pulses of equal amplitude and duration (23 ns) were used to generate the primary echo signal. The nominal angle of the resonant spin rotation was $2\pi/3$. The pulse separation varied from 300−

(12) Scheidt, W. R. Personal communication.
(13) Byrn, M. P.; Katz, B. A.; Keder, N. L.; Levan, K. R.; Magurany, C. J.; Miller, K. M.; Pritt, J. W.; Strouse, C. E. *J. Am. Chem. Soc.* **1983**, *105*, 4916.
(14) Mailer, C.; Taylor, C. P. S. *Can. J. Biochem.* **1972**, *50*, 1048.
(15) Turner, D. L. *Eur. J. Biochem.* **1995**, *227*, 829.
(16) Emerson, S. D.; La Mar, G. N. *Biochemistry* **1990**, *29*, 1556.
(17) Banci, L.; Pierattelli, R.; Turner, D. L. *Eur. J. Biochem.* **1995**, *232*, 522.
(18) La Mar, G. N.; Chen, Z.; Vyas, K.; McPherson, A. D. *J. Am. Chem. Soc.* **1995**, *117*, 411.
(19) (a) Quinn, R.; Valentine, J. S.; Byrn, M. P.; Strouse, C. E. *J. Am. Chem. Soc.* **1987**, *109*, 3301. (b) Soltis, S. M.; Strouse, C. E. *J. Am. Chem. Soc.* **1988**, *110*, 2824. (c) Innis, D.; Soltis, S. M.; Strouse, C. E. *J. Am. Chem. Soc.* **1988**, *110*, 5644.
(20) Keller, R. M.; Wüthrich, K. *Biochim. Biophys. Acta* **1972**, *285*, 326.
(21) (a) Williams, G.; Clayden, N. J.; Moore, G. R.; Williams, R. J. P. *J. Mol. Biol.* **1985**, *183*, 447. (b) Veitch, N. G.; Whitford, D.; Williams, R. J. P. *FEBS Lett.* **1990**, *269*, 297.
(22) McLachlan, S. J.; La Mar, G. N.; Lee, K.-B. *Biochim. Biophys. Acta* **1988**, *957*, 430.
(23) Oosterhuis, W. T.; Lang, G. *Phys. Rev.* **1969**, *178*, 439.
(24) Safo, M. K.; Gupta, G. P.; Walker, F. A.; Scheidt, W. R. *J. Am. Chem. Soc.* **1991**, *113*, 5497.
(25) Takenaka, A.; Sasada, Y.; Watanabe, E.-I.; Ogoshi, H.; Yoshida, Z.-I. *Chem. Lett. Jpn.* **1972**, 1235.
(26) Shokhirev, N. V.; Walker, F. A. *J. Am. Chem. Soc.* **1998**, *120*, 981 (accompanying paper).
(27) Borbat, P.; Raitsimring, A. New Pulse EPR Spectrometer at the University of Arizona, In *Abstracts of 36th Rocky Mountain Conference on Analytical Chemistry*; Denver, CO, July 31-August 5, 1994; sponsored by Rocky Mountain Section, Society for Applied Spectroscopy and Colorado Section, American Chemical Society; p 94.

400 ns to 1900−2200 ns, with 10 ns steps. The phase relaxation rate for these samples happens to be rather fast, namely 1.3×10^6 s^{-1}, and the amplitude of the signal decays by an order of magnitude at a pulse separation of 900 ns. Due to this experimental fact, to keep a feasible signal/noise ratio and to utilize the initial surplus of signal amplitude, and thus to cover as much pulse separation as possible and to ensure high resolution in further Fourier transforms, we performed the data acquisition in two stages. Mainly, we used two 1000 ns time intervals with a 200 ns overlap. In the second time interval the attenuation of the signal was set to zero. These two parts of the time domain data were then assembled into one array after adjusting them by the known attenuation. The 200 ns overlap in these two parts was used as an additional control on the performance of stitching together the time domain kinetics. The number of accumulations at each step of data collection was generally 1000−4000 at a boxcar gate width of 15 ns. To avoid signal saturation the pulse repetition rate was no more than 400 Hz. Such measurements were performed at various field positions of the EPR spectrum in steps of 10−100 G. ESEEM spectra were obtained by Fourier transformation (FT) of the experimental time domain data. Before the FT procedure the time domain data were subjected to band-pass or rejecting filtration with a filter, constructed by Dr. Astashkin,[28] and normalization. For normalization, the decay function was approximated by a second-order polynomial, which was fit in semilogarithmic coordinates through the experimental data by means of the least-squares method. The decay function obtained was subtracted from the experimental data (in semilogarithmic coordinates), yielding the nonmodulated part of the signal normalized to unity. These decay functions were found to be virtually exponential over the available time range and only slightly depended on field position. The uncertainty in measurement of spectral peak position in the FT ESEEM spectra was one or two steps of frequency domain quantization, depending on line shape, i.e., 0.05−0.1 MHz. The normalized noise level (for unit signal) in the FT spectra at the given experimental conditions was about $\pm 3 \times 10^{-3}$, and this value defines the accuracy of the amplitude measurements. In some cases the normalized modulation amplitude was measured directly in the time domain, yet filtration was also applied.

Theory

Analysis of the magnetic field strength dependences of the frequency shifts and amplitudes of sum combinational lines is based on comparison of the experimental spectra to those simulated for particular ligand orientations. To provide a background for the data processing and simulations that follow, we start with brief excerpts from ESEEM theory. Two fundamental frequencies, ν_α and ν_β, of a system which contains an electron spin $S = {}^1/_2$ and a nuclear spin $I = {}^1/_2$ are described by the following expression:[29−32]

$$\nu_{m_s} = |\vec{\mathbf{h}}^{\pm}| \qquad \vec{\mathbf{h}}^{\pm} = -\nu_I \mathbf{l} + \frac{\mathbf{Dgl}}{g_e} m_s \tag{1}$$

$$\nu_{m_s} = [(m_s A_1 - \nu_I l_1)^2 + (m_s A_2 - \nu_I l_2)^2 + (m_s A_3 - \nu_I l_3)^2]^{1/2}$$

where $m_s = \pm {}^1/_2$ for α or β electron spins, respectively, **D** is the tensor of the hyperfine interaction (HFI), **g** is the **g** tensor, ν_I is the nuclear Larmor frequency at a given magnetic field $\mathbf{B_m}$ and **l** is a unit vector which coincides with the direction of the external magnetic field $\mathbf{B_m}$. The particular form of A_i depends on the reference coordinate frame (RCF) in which they are calculated. For systems where **g** tensor anisotropy exceeds the anisotropy of the hyperfine interaction (HFI), the convenient RCF is that in which the axes coincide with the principal axis of the **g** tensor. In this RCF, with HFI caused by dipolar (in the point−dipole approximation)[9,33] and isotropic hyperfine interaction, the other terms of eq 1 are defined as

$$l_1 = \sin\theta\cos\phi \qquad l_2 = \sin\theta\sin\phi \qquad l_3 = \cos\theta$$

$$A_i = T \times [g_i l_i (g_i (3n_i^2 - 1) + a/T) + \sum_{k \neq i} 3 g_k^2 l_k n_i n_k]/g_e \tag{2}$$

$$n_1 = \sin\theta_n \cos\phi_n \qquad n_2 = \sin\theta_n \sin\phi_n \qquad n_3 = \cos\theta_n$$

where n_i are the direction cosines of the radius-vector **r** connecting the electron and nuclear spins in the RCF, a is the isotropic hyperfine coupling constant, g_i are the principal values, and $T = -\beta_e\beta_n g_n/\hbar r^3$, β_e = Bohr magneton, β_n = nuclear magneton, r = electron−nuclear distance.

The modulation of the primary ESE consists of two fundamental frequencies, ν_α and ν_β determined by eq 1, as well as their sum and difference combinations: $\nu_\pm = \nu_\alpha \pm \nu_\beta$. In this work we are particularly interested in the sum combinational line and in the case of weak hyperfine interaction. To give an idea of how the position of this line depends on the orientation of the nuclei in the RCF, let us consider a particular orientation of the magnetic field in the RCF, e.g., the magnetic field along the z axis, $l_3 = 1$, $l_1 = l_2 = 0$. For this particular case, as follows from eq 1 (see also ref 7):

$$\nu_{\alpha,\beta} = \sqrt{(\nu_I \pm A_3/2)^2 + (A_2^2/4) + (A_1^2/4)}$$
$$\nu_+ \approx 2\nu_I + \frac{A_1^2 + A_2^2}{4\nu_I} = 2\nu_I + \frac{(3 g_3 T \sin\theta_n \cos\theta_n)^2}{4\nu_I} \tag{3}$$

As one can see from eq 3, for weak hyperfine interaction, the shift of ν_+ from $2\nu_I$ is positive and reaches a maximum when the angle between the z axis of the RCF and r is 45°. The maximal value of the shift therefore is equal to $(3g_3T)^2/16\nu_I$, and, for instance, the near protons of the ligands (distance from Fe(III) ~3 Å, $\theta_n \sim 42°$) should demonstrate a line shifted from double the proton Larmor frequency by ~1 MHz; for the distant protons of the OEP ring this shift is evaluated as 0.05 MHz, a value that would be almost undetectable.

The modulation of the primary spin−echo signal $v(\tau)$ for this spin system and a particular orientation of electron and nuclear spins is described by the expression:[34]

$$v(\tau) \propto 1 - (k/2)[1 - \cos 2\pi\nu_\alpha\tau - \cos 2\pi\nu_\beta\tau + ({}^1/_2)\cos(2\pi\nu_-\tau) + ({}^1/_2)\cos(2\pi\nu_+\tau)] \tag{4}$$

If the system contains (i) nuclei, the resulting primary spin−echo kinetics is a product of such individual kinetics $v^{(i)}(\tau)$.[34]

$$V(\tau) = \prod_{(i)} v^{(i)}(\tau) \tag{5}$$

This expression immediately demonstrates that a multinuclear system will generate a set of harmonics as a result of cosine multiplication. Amplitudes of these harmonics are half the

(28) Astashkin, A. V.; Kawamori, A. *J. Magn. Resonan., Ser. A* **1995**, *112*, 24.
(29) Hutchinson, C. A.; McKay, D. B. *J. Chem. Phys.* **1977**, *66*, 3311.
(30) (a) Henderson, T. A.; Hurst, J. C.; Kreilick, R. W. *J. Am. Chem. Soc.* **1985**, *107*, 7299. (b) Hurst, J. C.; Henderson, T. A.; Kreilick, R. W. *J. Am. Chem. Soc.* **1985**, *107*, 7294.
(31) Hoffmann B. M.; Martinsen, J.; Venters, R. A. *J. Magn. Reson.* **1984**, *110*, 59.
(32) Iwasaki, M.; Toriyama, K. In *Electronic Magnetic Resonance of the Solid State*; Weil, J. A., Bowman M. K., Morton J. R., Preston K. F., Eds.; Canadian Society of Chemistry: Ottawa, 1987; p 545.
(33) Dikanov, S. A.; Spoyalov, A. P.; Hüttermann, J. *J. Chem. Phys.* **1994**, *100*, 7973.

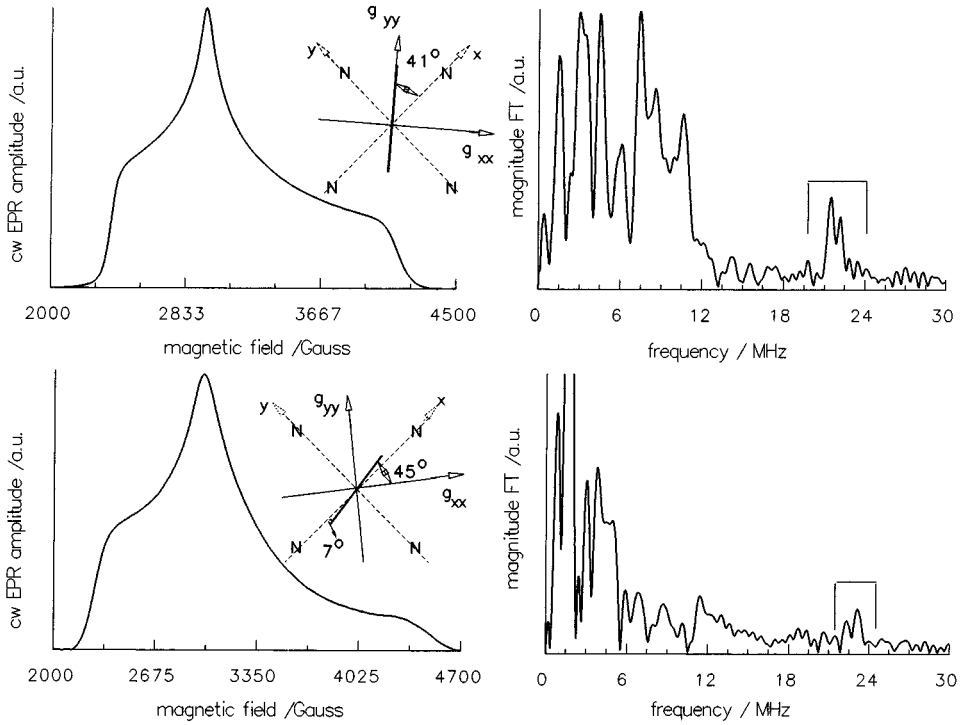

Figure 1. (Left column) CW EPR spectrum of 10^{-3} M $[OEPFe(4\text{-}NMe_2Py)_2]^+Cl^-$ in a 1:2 methylene chloride-d_2/toluene-d_8 glass (top) and $[OEPFe(ImH)_2]^+Cl^-$ in a 3:1 dimethylformamide-d_7/acetonitrile-d_3 glass (bottom), each at 77 K. Microwave power: 0.1 mW. Observed g values: $g_1 = 2.85$, $g_2 = 2.28$, $g_3 = 1.63$ (top); $g_1 = 2.97$, $g_2 = 2.25$, $g_3 = 1.49$ (bottom). Insets: Orientation of the axial ligand planes in each complex, along with the orientation of the in-plane **g** tensor components g_{xx} (smallest) and g_{yy} (largest) determined in this work. (Right column) FT-ESEEM spectra (primary echo) of the same complexes at a magnetic field of 2500 G (top) and 2640 G (bottom). Open square marks the $I(\nu_+)$. Lines in the frequency interval 0−12 MHz are caused by interaction of the unpaired electron of Fe(III) with N, D, and H nuclei. Microwave frequency: 8.702 GHz for top spectrum and 8.804 GHz for bottom spectrum. Temperature: 4.2 K. τ step: 10 ns. Time interval: 360−2160 ns. Nominal angle of resonant spin rotation: $2\pi/3$. Pulse duration: 23 ns.

product of the amplitudes at the basic frequencies that generate the particular harmonic. As follows from eq 4, the modulation amplitude (or intensity of the FT ESEEM spectrum) is proportional to the parameter k. This parameter is the product of allowed and forbidden transition probabilities and, in the same approximation as was applied for deriving the fundamental frequencies, $k = \sin^2 \eta$, where $\cos \eta$ is determined by the following expression:[35]

$$\cos \eta = \frac{\vec{\mathbf{h}}^+\vec{\mathbf{h}}^-}{|\vec{\mathbf{h}}^+||\vec{\mathbf{h}}^-|}$$
$$\vec{\mathbf{h}}^\pm = \left[\left(\frac{A_1}{2} \pm \nu_I l_1\right), \left(\frac{A_2}{2} \nu_I l_2\right), \left(\frac{A_3}{2} \pm \nu_I l_3\right)\right] \quad (6)$$

The explicit expression for k as derived from eq 6 is[9]

$$k = \frac{\nu_i^2}{\nu_\alpha^2 \nu_\beta^2}\{[A_1 l_2 - A_2 l_1]^2 + [A_2 l_3 - A_3 l_2]^2 + [A_1 l_3 - A_3 l_1]^2\} \quad (7)$$

or the case of an isotropic **g** tensor, i.e., when $g_1 = g_2 = g_3$, eq 7 transforms to the well-known result often used for analysis of ESEEM spectra:[37]

$$k = \frac{\nu_i^2 B^2}{\nu_\alpha^2 \nu_\beta^2} \qquad B = 3gT \sin\theta \cos\theta \qquad \theta = \boldsymbol{r} \wedge \boldsymbol{1} \quad (8)$$

In a disordered (or partially disordered) system, each given magnetic field $\mathbf{B_m}$ represents not a unique, but a set of orientations, and consequently a set of fundamental, sum and difference frequencies. Because the modulation amplitude also depends on orientation, eq 5 for this system must be rewritten as

$$\langle V(\tau)\rangle \propto \langle \prod_{(i)} v^{(i)}(\tau)\rangle \quad (9)$$

where $\langle ... \rangle$ means averaging over orientations. The allowed orientations are determined by the given field position, individual line shape, and **g** tensor. Equation 9 was straightforwardly used for simulations, as described in the Simulutation Section.

Results

The cw EPR spectra of $[OEPFe(L)_2]^+Cl^-$ obtained in this work are identical with those reported previously,[24,36] Figure 1, left panels. These paramagnetic centers are each characterized by a rhombic **g** tensor with principal values of 2.85, 2.28, 1.63 and 2.97, 2.25, 1.49 for L = 4-NMe_2Py and ImH, respectively. The FT ESEEM spectra are in general similar to published spectra of low-spin iron porphyrinates and consist of numerous lines caused by interaction of the electron spin with nitrogen, deuterium, and proton nuclei of the molecule and the solvent. A representative example of such a spectrum is shown in Figure 1, right panel. The whole spectrum covers the

(34) Mims, W. B. *Phys. Rev. B* **1972**, *5*, 2409.
(35) Carrington, A.; McLachlan, A. D. *Introduction to Magnetic Resonance with Application to Chemistry and Chemical Physics*; Harper and Row: New York, 1967; Chapter 7.
(36) Walker, F. A.; Reis, D.; Balke, V. L. *J. Am. Chem. Soc.* **1984**, *106*, 6888.
(37) Dikanov, S. A.; Tsvetkov, Yu. D. *Electron Spin−Echo Envelope Modulation (ESEEM) Spectroscopy*; CRC Press: Boca Raton, Florida, 1992; Chapter 13.

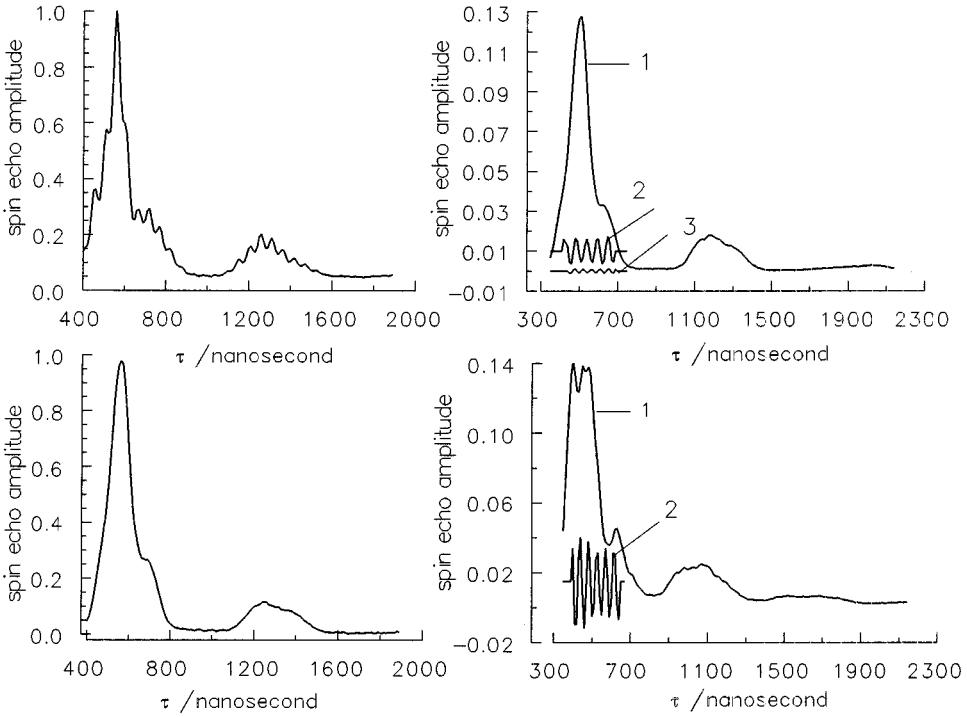

Figure 2. Primary ESEEM and normalized DP proton modulation of $[OEPFe(III)(L)_2]^+$: (left panel, $\mathbf{B_m}$ = 2100 G; (top) L = h_4-Im; (bottom) L = d_4-Im; right panel: (top) L = d_4-Im, B_m = 2140 G, (1) primary ESEEM, (2) normalized DP modulation, (3) noise; (bottom) L = d_4-Im, $\mathbf{B_m}$ = 2640 G, (1) primary ESEEM, (2) normalized DP proton modulation. Microwave frequency: 8.804 GHz. Temperature: 4.2 K. Step: 10 ns. Nominal angle of resonant spin rotation: $2\pi/3$. Pulse duration: 23 ns.

frequency range from 0 to 25−30 MHz (the upper limit depends on magnetic field). In this paper, as was mentioned in the Introduction, we are concentrating on a part of this spectrum, the proton sum combination line, $I(\nu_+)$, which is located in the vicinity of twice the proton frequency, $2\nu_H$. As one can see from Figure 1, the $I(\nu_+)$ signal is well-separated from the rest of the spectrum, which allows one to apply a rather wide band-pass filter without acquiring the outside lines. It should be noted that the reason that two-pulse ESEEM experiments have been utilized in this work is that we wished to obtain quantitative intensity data from the spectra; multipulse ESEEM pulse trains entail significant signal intensity losses and very cumbersome normalization procedures.

As already mentioned, $[OEPFe(ImH)_2]^+Cl^-$ was prepared with imidazole-d_4 and -h_4. It was expected that the imidazole-d_4 sample would show proton modulation only from the distant protons (DP) of the OEP ring and the imidazole-h_4 sample would demonstrate proton modulation caused by the DP of both the OEP and the imidazole ligands, and the NP of the imidazoles. Indeed, the expected difference in the modulation patterns of these two compounds is readily seen in the time domain directly, Figure 2, left panel, without any additional data processing. The sample with imidazole-d_4 hardly shows any visible proton modulation and depicts very deep deuterium modulation. On the other hand, the sample with imidazole-h_4 demonstrates deep proton modulation, and, at the same time, a large decrease in the depth of the deuterium modulation. It can be readily concluded from these preliminary observations that the differences in modulation patterns of these two samples are caused by NP(ND) of imidazole; the DP(DD) are too far from Fe(III) to cause such variations. As we have shown previously,[9] the magnetic field dependence of the modulation amplitude of the DPs allows one to unambiguously determine the ordering of the g values. Therefore, to obtain this ordering for $[OEPFe(ImH)_2]^+$, measurements on the imidazole-d_4 sample were performed first at various field positions in the range of 2100 < $\mathbf{B_m}$ < 3000 G (2.99 < g < 2.1). As can be seen in Figure 2, the ESE signal in this sample is modulated, at least at lower fields, to zero over substantial time intervals, with a corresponding loss of DP modulation in these intervals. In such situations it was not possible to use directly the method of extracting the proton modulation, described in the Experimental Section (i.e., filtration/normalization/FT), because the zero part of the signal causes an uncertainty in the resulting modulation amplitude. To avoid such complications and ambiguities in determining the DP modulation amplitude a modified procedure was applied which still exploits filtration and also acquires a priori knowledge of the properties of the sum combination modulation, discussed elsewhere,[37] namely: (1) the frequency of the DP modulation does not exceed double the proton frequency by more than 0.1−0.15 MHz, (2) the characteristic time of damping for this modulation is more than 5−10 μs, and (3) this modulation is weak—that is, its normalized amplitude <<1. Therefore, at least during the first 1 μs, the observed spin−echo signal, $V(\tau)$ may be presented as a product of ESEEM at ν_+ , $V''(\tau)$, and at all others frequencies, $V'(\tau)$, in accord with eq 9 above:

$$V(\tau) = V'(\tau)\, V''(\tau) \qquad V''(\tau) = 1 + a\cos(2\pi\nu_+\tau)$$

where a is the DP modulation amplitude. A narrow band rejecting filtration of $V(\tau)$ at the ν_+ frequency yields $V'(\tau)$ and subsequently the DP modulation

$$1 + a\cos(2\pi\nu_+\tau) = [V(\tau)/V'(\tau)]$$

The modulation amplitude is then directly read in the time domain, using the average value of 3−4 periods of modulation in the first microsecond of data acquisition, where the ESE signal substantially exceeds the noise level. [Note: Extracting the modulation amplitude from the time domain data is not a novelty

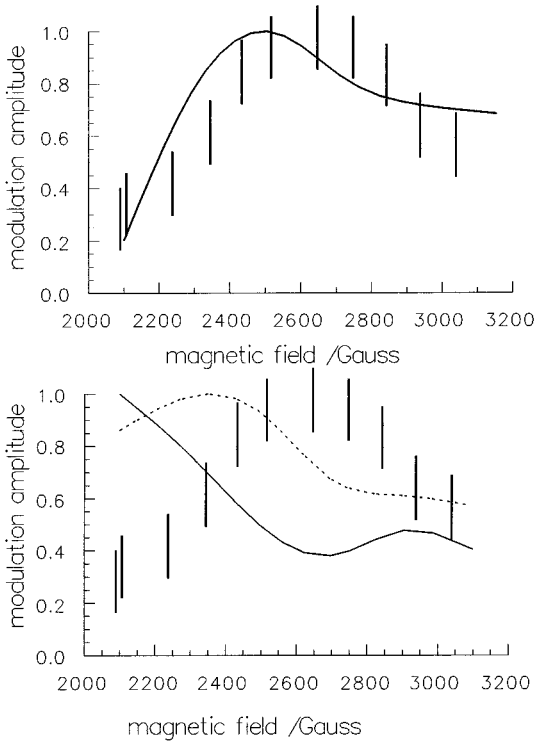

Figure 3. Experimental (bars) and calculated (lines) magnetic field dependence of DP modulation amplitude for $[OEPF(d_4\text{-Im})_2]^+$. The calculated dependences correspond to $g_{zz} > g_{yy} > g_{xx}$ (top) and $g_{xx} > g_{yy} > g_{zz}$ (bottom). In the last case vectors connecting each pair of four 4.3 Å protons of the OEP ring coincide with the *x* and *y* axes of the RCF (dashed line) or make 45° (135°) angles with these axes (solid line).

in ESEEM and was widely used in the 1970s.[38] However, such an "old fashioned" approach could not be directly applied in this particular case because of very weak proton modulation, yet it works in combination with modern filtering techniques.] To optimize the width of the filter and to examine its response to signal/noise ratio we performed extensive applications of this procedure to simulated time domain patterns which imitated the experimental ESEEM data and included the noise and relaxation decay as well. It was found that the optimal width of the filter which does not distort the modulation amplitude and does not pick up additional noise is about 0.25 MHz. The minimal normalized modulation amplitude which still can be extracted at the given experimental conditions is about 0.4%; this limit is determined by the noise level and the accuracy in zero line subtraction. Figure 2, right panel, shows representative results of the application of the above procedure to the experimental data. Pattern 3, presented in Figure 2, right panel, gives an idea of the noise level. The noise curve was obtained with the filter centered at $2\nu_I + 6.6$ MHz, where the amplitude of the combinational harmonics of ν_+ and ν_D was definitely below noise level. The resulting dependence of DP modulation amplitude on magnetic field $\mathbf{B_m}$ is shown in Figure 3 and the maximal amplitude of DP modulation was found to be about 2%. This is a bell-shaped curve, which, as we demonstrated previously,[9] corresponds to the "normal order" of *g* values, $g_{zz} > g_{yy} > g_{xx}$. More details are found in the Simulation section below. Before proceeding with this, we allow ourselves two remarks. First, it is easy to demonstrate that the position of the DP line coincides with double the proton frequency. For this purpose one may apply the well-known method of adding the same constant to $V(\tau)$ and $V'(\tau)$ (constant $>> V(\tau)$), which eliminates peculiarities caused by the zero amplitude parts of the signal, yet distorts the magnitude of the FT. Having used this procedure it was found that the DP lines are, indeed, situated at double the proton frequency. Second, the procedure used here for extracting the modulation of the DPs is similar to the "quotient" method introduced by Mims and Peisach for analysis of ESEEM spectra[39] for extracting a particular normalized modulation from a complicated pattern, and then widely used elsewhere.[40] The suggested procedure might be dubbed the "numerical quotient method" and used for analysis of narrow lines of known position.

The $[OEPFe(h_4\text{-Im})_2]^+$ data were processed as described in the Experimental Section. Representative example of the $I(\nu_+)$ at various magnetic fields, $\mathbf{B_m}$, are shown in Figure 4. Depending on field position the $I(\nu_+)$ is either a one line or two line pattern, and is surrounded by harmonics whose positions are close to $\nu_+ \pm \nu_D$ and $\nu_+ \pm 2\nu_D$, where ν_D is the Larmor frequency of deuterium. The position of the maximum of the one line that is observable at $2500 < \mathbf{B_m} < 2800$ G is very close to $2\nu_H$ (the shift from $2\nu_H$ does not exceed 0.1 MHz), and its intensity is close to the proton modulation amplitude observed in the imidazole-d_4 sample. Therefore this line may be assumed to originate from the interaction of the electron spin with the DP of the OEP ring and the four DP of imidazole. The second line is substantially shifted from $2\nu_H$. As is well-known, (see, e.g., ref 7 and eq 3 in the Theory section) the shift is caused by the strongly anisotropic hyperfine interaction; therefore this line originates from the interaction of low-spin Fe(III) and the NP of imidazole. The peak intensity of this line and the shifts were found to depend on the strength of the magnetic field, $\mathbf{B_m}$. These dependences were carefully investigated across the EPR spectrum of the Fe(III) complex, in the range $2100 < \mathbf{B_m} < 3100$ G (or $3 > g > 2.07$), and they are presented in Figure 5. As demonstrated previously,[9] this field (*g* value) interval is quite informative for determination of the order of *g* values and ligand orientations, and little is gained by continuing the measurements toward the extreme high field end of the EPR spectrum, where *g* strain causes severe broadening and diminution of the ESEEM signal. Over this field interval, as is shown in Figure 5, the peak magnitude of $I(\nu_+)$ varies by approximately a factor of 5. It reaches a maximum (16% of the normalized amplitude) at the extreme low field position, $\mathbf{B_m} = 2100$ G, and levels off at 3.0−3.5% at $\mathbf{B_m} \approx 2600$ G. The shift Δ starts from a maximal value of 0.8 MHz at the extreme low field position, and decreases gradually to 0.2 MHz at $\mathbf{B_m} = 3100$ G.

Similar measurements were performed for $[OEPFe(4\text{-}NMe_2\text{-}Py)_2]^+$, but the deuterated analogue of the axial ligand was not available. In general, the results are similar to those obtained for $[OEPFe(ImH)_2]^+$, but differ in details. The particulars of the data processing for this complex are shown in Figure 6. One starts with the original time domain data (Figure 6a), then applies filtration and decay adjustments (Figure 6b,c), and follows with Fourier transformation, which produces the $I(\nu_+)$, (Figure 6d). Depending on the magnetic field position the $I(\nu_+)$ is again either a single line, Figure 6d, or two lines, Figure 7. The first line, whose position is very close to $2\nu_H$ ($(\nu_+ - 2\nu_H) \leq 0.1$ MHz), becomes observable at $\mathbf{B_m} > 2400$ G and its maximal absolute magnitude (at $\mathbf{B_m} \approx 2500$ G) is about twice

(38) (a) Szajdzinska-Pietek, E.; Malonado, R.; Kevan, L.; Berr, S.; Jones, J. *J. Phys. Chem.* **1985**, *89*, 1547. (b) Yudanov, V. F.; Grishin, Yu. A.; Tsvetkov, Yu. D. *Zh. Strukt. Khim.* **1975**, *16*, 747. (c) Dikanov, S. A.; Yudanov, V. F.; Tsvetkov, Yu. D. *Zh. Strukt. Khim.* **1978**, *19*, 245.

(39) Mims, W. B.; Peisach, J. In *Advanced EPR: Applications in Biology and Biochemistry*; Hoff, A. J., Ed.; Elsevier: New York, 1989; pp 1−57.

(40) Warncke, K.; McCracken, J. *J. Chem. Phys.* **1995**, *103*, 6829.

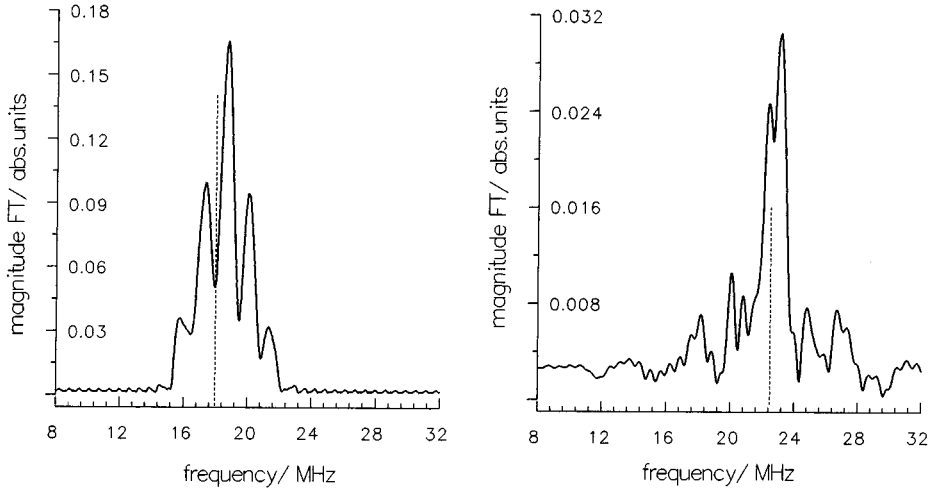

Figure 4. Experimental normalized sum combinational lines, $I(\nu_+)$ of $[OEPFe(h_4\text{-}Im)_2]^+$: $\mathbf{B_m}$ = 2100 G (left) and 2640 G (right). Dotted line marks the position of $2\nu_H$ for these particular experiments.

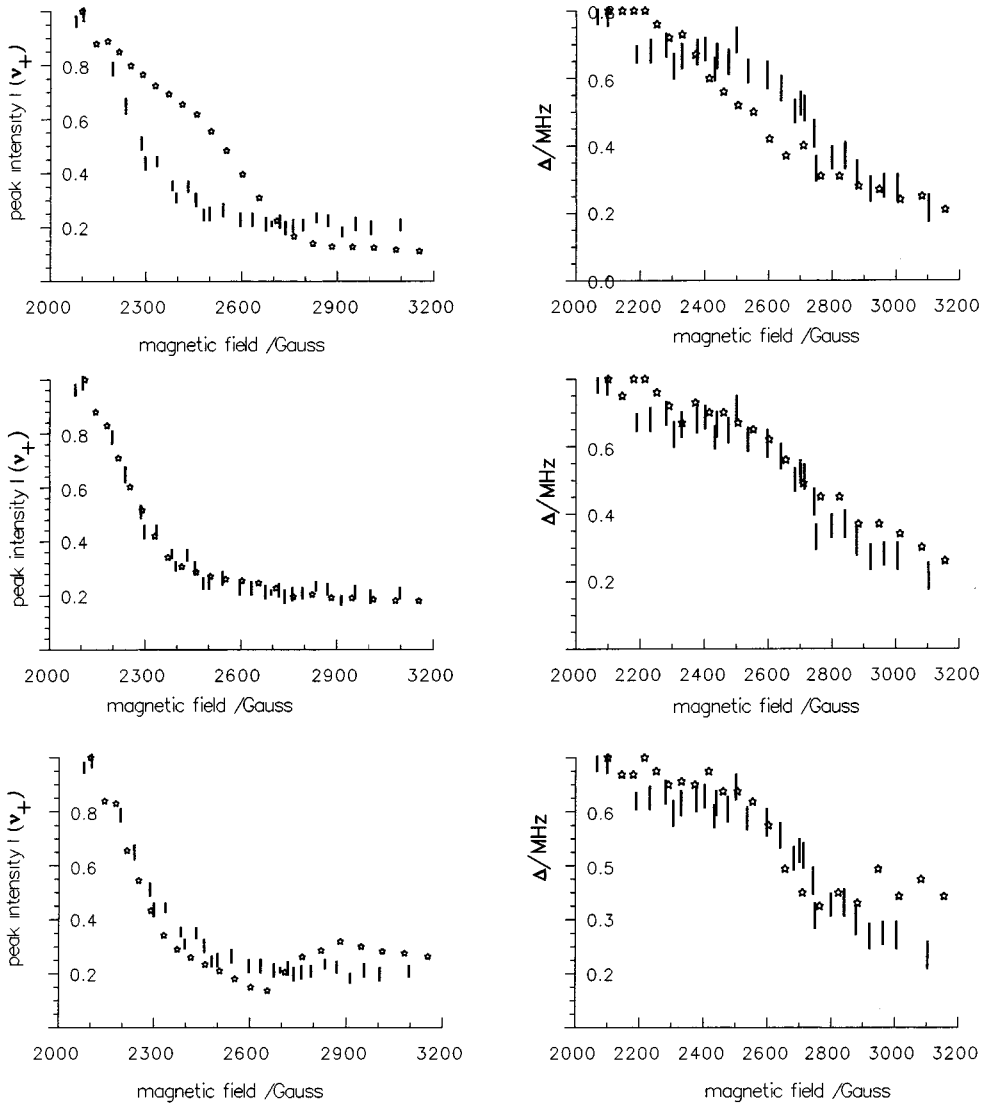

Figure 5. Experimental (bars) and calculated (stars) magnetic field strength dependences of the relative amplitudes and shifts of the NP peaks of $[OEPFe(ImH)_2]^+$: in all calculations $g_{zz} > g_{yy} > g_{xx}$; (top row) $x \parallel$ LP; (bottom row) $x \perp$ LP; (middle row) angle between x and perpendicular to LP is 45°. Fe−proton distances, r = 3.2 Å, $r-z$ axis angle = ±41°. Other details of simulation and parameters used are described in the Simulation section.

as large as that found in the imidazole case. The dependence of the peak intensity of this line on $\mathbf{B_m}$, investigated over the range 2400 < $\mathbf{B_m}$ < 3000 G, is shown in Figure 8, where it is seen that its magnitude varies by a factor of 1.6−1.8 over the magnetic field range investigated, reaching a maximum at 2400−2500 G (≈4−4.5% of the normalized amplitude). We

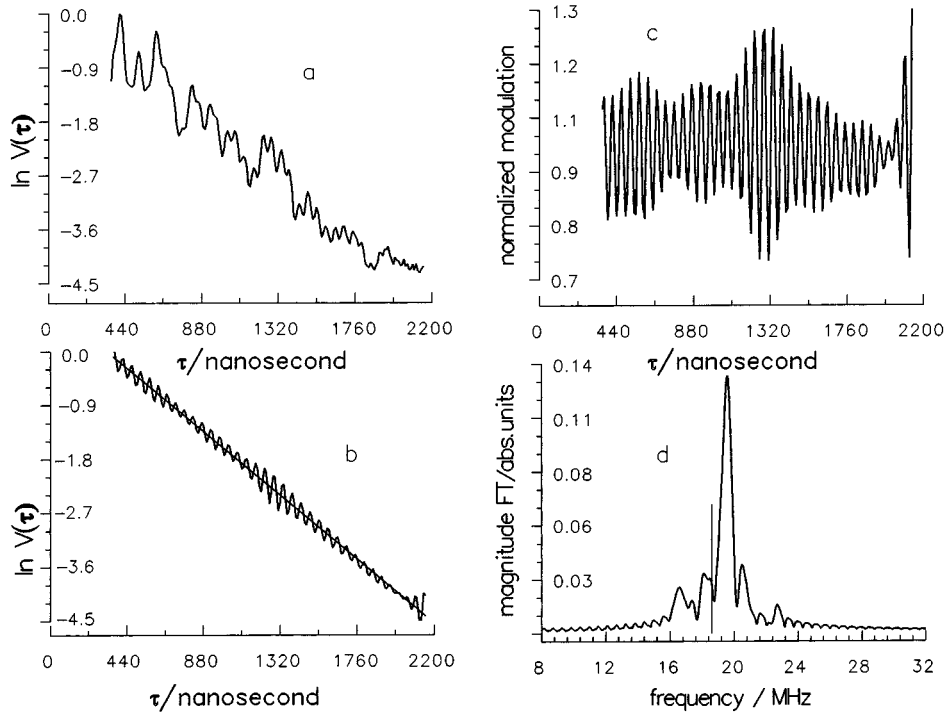

Figure 6. The sequence of experimental data processing to obtain the normalized $I(\nu_+)$: (a) initial primary ESEEM time-domain data; (b) time-domain data resulting from a) after applying band-pass filtration, bandwidth of filter ±5 MHz at $2\nu_H$ (solid line is the decay function used); (c) normalized time domain data resulting from b after subtracting the decay function and exponentiating the residual; (d) the $I(\nu_+)$ resulting from magnitude FT of c (thin line marks the position of $2\nu_H$ in this particular experiment). $\mathbf{B_m}$ = 2182 G; other parameters are the same as those for Figure 1, right column, top.

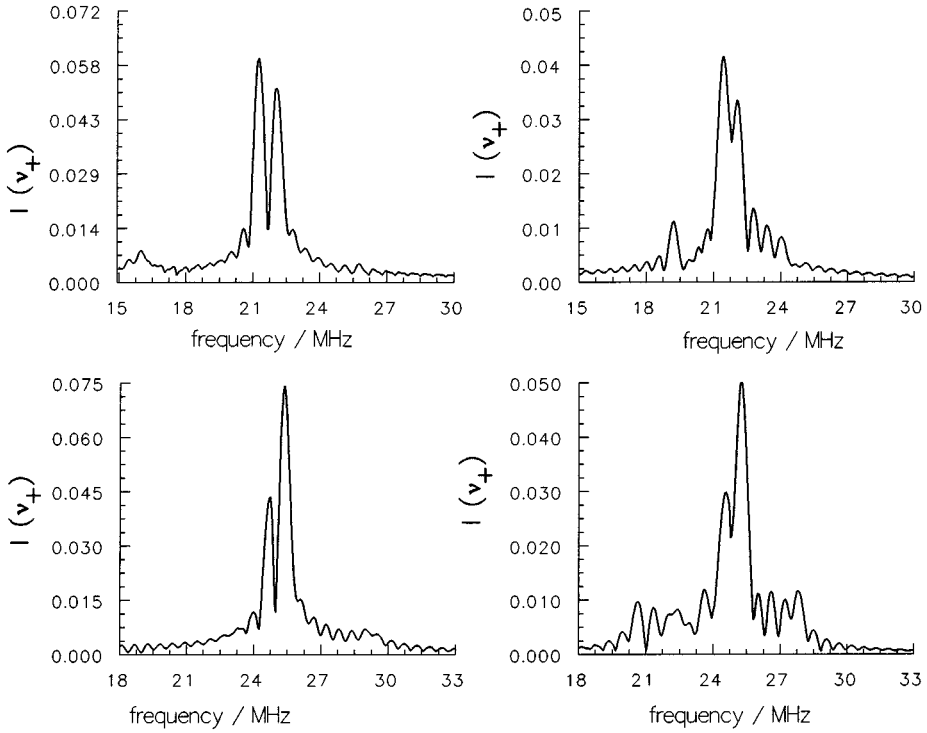

Figure 7. Experimental (right column) and simulated (left column) normalized proton sum combinational line, $I(\nu_+)$ of $[OEPFe(4\text{-}NMe_2Py)_2]^+$. $\mathbf{B_m}$ = 2500 and 2900 G for top and bottom row, respectively. Simulations: x ⊥ LP, $g_{zz} > g_{yy} > g_{xx}$, Fe−NP distances, r = 3.1 Å, r−z axis angle ±41°. DP coordinates are taken from ref 24. Other details of the simulations and parameters are described in the Simulation section.

were not able to use this dependence explicitly for determination of the g ordering with respect to ligand orientation, because the important part of this dependence at the low-field end of the EPR spectrum is not available, since the DP signal is obscured by harmonics. However, we can use it implicitly for these purposes by utilizing the just mentioned finding that the intensity of the line is approximately double that for $[OEPFe(ImH)_2]^+Cl^-$ in the range of 2400−2900 G. It was found from the simulations (see Figure 9), that at specific orientations of the ligands, the NP lines have a shoulder at $2\nu_I$ that adds intensity at the DP line position. More details are found in the Simulation and Discussion sections. For the second

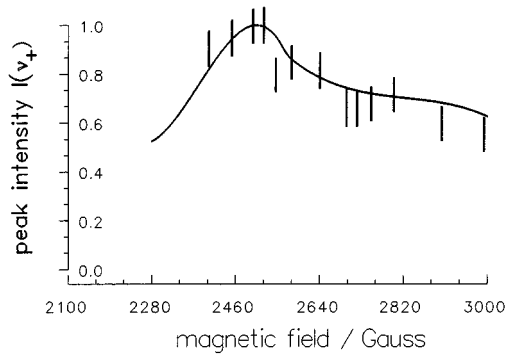

Figure 8. Experimental (bars) and calculated (line) magnetic field strength dependence of the relative peak amplitude at $2\nu_H$ for $[OEPFe(4\text{-}NMe_2Py)_2]^+$. $x \perp$ LP, $g_{zz} > g_{yy} > g_{xx}$. Other details of simulation and parameters are described in the Simulation section.

line, the dependences of the peak intensity and shift were investigated across the EPR spectrum of the Fe(III) complex in the range $2180 < \mathbf{B_m} < 3000$ G (or $2.85 > g > 2.07$). Over this field interval, as is shown in Figure 10, the peak magnitude of this part of $I(\nu_+)$ varies by approximately a factor of 5. It reaches a maximum (≈13% of the normalized amplitude) at the extreme low field position, $\mathbf{B_m} = 2180$ G, a minimum (≈3%) at $\mathbf{B_m} = 2500$ G, and increases again (up to 5−5.5%) with further magnetic field increase. The shift starts from a maximal value of 0.9 MHz at the extreme low field position, decreases to 0.5−0.55 MHz at $\mathbf{B_m} = 3000$ G, and shows a shallow minimum of 0.4 MHz at 2650−2700 G.

Thus, the output of the experiments was the magnetic field dependences of the $I(\nu_+)$ maxima and their shifts. Because a particular field position selects only certain orientations of molecules, the observed dependences can be used to obtain structural information. The methods of analysis of the experimental data to obtain this information are described in the following sections.

Simulations

(1) Parameters. As follows from theory, calculation of FT ESEEM spectra requires as input parameters $r^{(i)}$, $n_i^{(i)}$, a_i (the constant for the isotropic hyperfine interaction for the i-th proton), the principal values of the **g** tensor, $\mathbf{B_m}$, the microwave frequency, and the individual line shape function. OEP includes only DP, which may be separated approximately into three groups: four meso-H at a distance 4.3−4.4 Å, 16 methylene protons at 5.7−6.2 Å, and 24 methyl protons at distances of 6.5−7 Å. Vectors connecting the opposite pairs of 4.3−4.4 Å meso protons bisect the angle between the nitrogens of the porphyrin ring. All other protons fill practically uniformly the $x-y$ plane. ImH adds just four DP at a distance of 5 Å, whereas 4-NMe_2Py brings an additional four DP at a distance of 5 Å and 12 DP at a distance of 7−8 Å. All DP of the ligands are reasonably close to the perpendicular to the porphyrin ring. The crystal structure of the $[OEPFe(4\text{-}NMe_2Py)_2]^+$ complex[24] indicates that the axial ligands are aligned in parallel planes nearly bisecting pairs of nitrogens of the porphyrin ring (structure I). In accord with this structure, the distances from Fe(III) to the NP of the axial ligands are equivalent and equal to 3.0 Å. In our simulations we have varied this distance from 3.0 to 3.1 Å. The angles between z (the z axis is taken as perpendicular to the porphyrinate plane) and **r** of the NP of each ligand in the crystal structure are not equivalent and are equal to ±33° and ±50°.[24] We assume that in solution, the molecule should adopt a more relaxed and symmetrical structure than this, with equivalent NP distances and angles. Thus, in the simulations we have used the average angle between the **r** and z direction of ±41°. The direction cosines of the NP in the xy plane were varied in accord with the chosen RCF. We considered three RCF, where the z axis was always perpendicular to the plane of the porphyrin ring and (i) the x axis was parallel to the ligand plane (LP), ($x \parallel$ LP), (ii) perpendicular to the ligand plane ($x \perp$ LP), and (iii) 45° from the perpendicular to LP. The hyperfine constant for the NP was evaluated from NMR measurements[41] as −0.5 MHz. This constant was included in the simulations, although as is well-known[37] and as was confirmed by this group previously,[9] such small a values do not modify the magnetic field dependences of Δ and amplitude. Similar parameters were chosen for the NP of $[OEPFe(ImH)_2]^+$. However, because the observed shift for this sample was less than for $[OEPFe(4NMe_2\text{-}Py)^2]^+$ the distance was varied from 3.1 to 3.2 Å. As for the DP, in the simulations we included all DP with their coordinates as extracted from the crystal structure and recalculated in accord with the chosen RCF. The isotropic hyperfine coupling constant for the DP in all simulations was set to zero. The individual line-shape function $f(\mathbf{B_m} - \mathbf{B})$ of $[OEPFe(NMe_2Py)_2]^+Cl^-$, which includes such sources of broadening as g strain and hyperfine interaction, was chosen similar to that used previously,[9] based on the similarity of the EPR spectra of $[TPPFe(PzH)_2]^+Cl^-$ and $[OEPFe(NMe_2Py)_2]^+Cl^-$. As for $[OEPFe(ImH)_2]^+Cl^-$, where the observed line width was approximately twice that for $[OEPFe(NMe_2Py)_2]^+Cl^-$, the g strain broadening was increased correspondingly. For purposes of our calculations, the principal axis of the **g** tensor was set to coincide with that of the RCF. As for the order of principal g values, simulations were carried out for both $g_{zz} > g_{yy} > g_{xx}$ and $g_{xx} > g_{yy} > g_{zz}$.

(2) Simulation Technique. The numerical simulations of ESEEM spectra were performed in a manner similar to that described previously,[9] with the only difference being that calculations were made directly in the time domain instead of the frequency domain. (Both methods of simulation are strictly equivalent and differ only in technical details of program organization.) The method used in this paper is more convenient for data processing, although it requires more computational time. For simulation in the time domain at a particular magnetic field, the values of ν_α, ν_β, ν_+, ν_-, and k for (i)-nucleon were estimated by eqs 1, 2, and 7 for each allowed orientation and were directly fed into eq 4 to calculate partial ESEEMs. The resulting kinetics were obtained in accord with eq 9. To imitate the experiment, the same part of the simulated kinetics as acquired in the experiment was used for the FFT. Before Fourier transformation this part of the simulated kinetics was subjected to exactly the same treatment as were the experimental ones, i.e., filtration and normalization. Some of the simulated spectra $I(\nu_+)$ and the resulting dependences are shown in Figures 3, 5, and 7−10.

Discussion

Order of *g* Values. We start this discussion with an analysis of the order of the g values. For this purpose, in the previous work[9] the magnetic field dependence of the amplitude of the DP related line was utilized. It was demonstrated that the $g_{zz} > g_{yy} > g_{xx}$ order of g values leads to an increase in amplitude of the DP related part of $I(\nu_+)$ with increasing magnetic field from the low field extreme to higher magnetic field; the opposite order of g values gives the opposite result. Calculations of this type were performed for the DP of $[OEPFe(d_4\text{-}Im)_2]^+Cl^-$, where

(41) Watson, C. T. Ph.D. Thesis, University of Arizona, 1996.

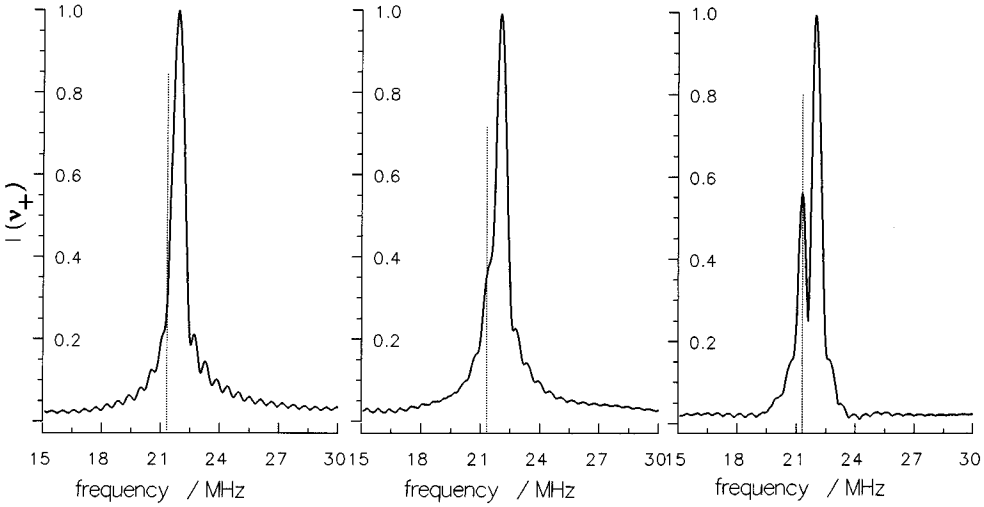

Figure 9. Simulated line shapes, $I(\nu_+)$, of $[OEPFe(ImH)_2]^+$ NP for various orientations of ligands in the RCF (left) $x \parallel$ LP; (right) $x \perp$ LP; (middle) 45° between perpendicular to LP and x. Unit for right spectrum is 4.6%. $\mathbf{B_m} = 2505$ G. The dashed line marks the position of $2\nu_H$ at this particular field.

the experimental magnetic field dependence of the DP intensity has been obtained. As was already mentioned, in this case only the DP of the OEP ring were considered. As was shown in the Theory section, the intensity of the DP, $I(\nu_+)$, depends on distance as r^{-6}. Therefore, four protons at a distance of 4.3−4.4 Å give approximately twice the intensity as 16 protons at distance of 5.7−6.2 Å; the addition to line intensity from the remaining 24 protons at distances of 6.5−7 Å is less than 25%.

As in the previous work[9] the $g_{zz} > g_{yy} > g_{xx}$ order of g values leads to an increase in amplitude of $I(\nu_+)$ with increasing magnetic field from the low-field extreme to higher magnetic field, Figure 3 (top); for the opposite order of g values two situations were considered: the vectors connecting the pairs of opposite 4.3−4.4 Å protons are aligned with the xy axes, or they are rotated by 45° relative to these axes. For the first case, at the extreme low field position the magnetic field direction coincides with one of these vectors and is perpendicular to the other; that gives a zero intensity of $I(\nu_+)$ for the 4.3−4.4 Å protons. The consecutive increase in intensity from these protons with increase in magnetic field is compensated by the decrease in the intensity of the remaining protons of the OEP ring and thus results in the dependence shown in Figure 3 (bottom, dashed line). For the second case, both groups of DP give a decrease in intensity (Figure 3, bottom, solid line). Comparing these three calculated dependences of DP $I(\nu_+)$ with the experimental data we can conclude that for $[OEPFe(d_4\text{-}Im)_2]^+$ the order of g values is $g_{zz} > g_{yy} > g_{xx}$. As was already mentioned, the intensities of the DP line of $[OEPFe(h_4\text{-}Im)_2]^+$ was found to be close to those of the d_4-Im sample (compare, e.g., 2 ± 0.3% and 2.4 ± 0.3% for maximal DP intensities measured for these samples). Indeed, based on the same r^{-6} dependence of intensity on distance one cannot expect that four additional 5 Å protons of h_4-Im add more than 20% to the intensity of the OEP ring DP, as is observed experimentally.

Orientation of g_{xx} and g_{yy}. For $[OEPFe(h_4\text{-}Im)_2]^+Cl^-$, using the obtained order of g values, simulations of shifts and intensities of the NP with magnetic field were performed to derive the orientation of the ligand planes relative to the RCF (or vice versa). The results are shown in Figure 5. The comparison of simulations and experiment allows us to conclude that more probably the x and y axes of the RCF and the perpendicular to the LP make angles of about ±45°. As one can see from Figure 5, the difference in simulations and experiment is more pronounced for $x \parallel$ LP than for $x \perp$ LP. However, the simulations also show, Figure 9, that the shape of the NP line is a singlet over the entire magnetic field range of 2100−3100 G if $x \parallel$ LP or x makes an angle of 45° with the perpendicular to the LP. It becomes a resolved doublet in the range of 2400−2800 G for $x \perp$ LP, with one component of this doublet situated at double the proton frequency. The intensity of the component of the NP line at double the proton frequency is comparable with those observed (or simulated) for the DP. Therefore, for the case of $x \perp$ LP one may observe a substantial increase (approximately twice) in intensity of the DP line for the protonated ligands in comparison with deuterated ones. The lack of such increase for the discussed case is an additional reason to rule out the $x \perp$ LP orientation. Hence, all lines of argument are most consistent with the x and y axes of the RCF making angles of about ±45° with the perpendicular to the LP.

On the other hand, in the case of $[OEPFe(NMe_2Py)_2]^+Cl^-$ we observed this approximately factor of 2 intensity increase of the line at double the proton frequency (the line of the DP) in the range of 2400−2900 G. The 24 protons from the methyl groups are 7−8 Å away from Fe(III) and the increase in intensity of the DP line due to these protons is negligible. The observed increase in intensity may occur, as mentioned above, because of the specific line shape of the NP for $x \perp$ LP and $g_{zz} > g_{yy} > g_{xx}$ (see Figure 9). Therefore, the relative comparison of the line intensities at double the proton frequency of these two compounds gave us the first clue for understanding the ligand orientation in $[OEPFe(NMe_2Py)_2]^+Cl^-$.

The confirmation of this statement is found in the comparison of the experimental NP intensity dependence on magnetic field with simulations which were performed for various orientations of the LP (see Figure 10). The experimental NP intensity dependence on magnetic field shows a characteristic feature: a minimum at $\mathbf{B_m} \approx 2500$ G. This feature is reproduced in simulations only if $x \perp$ LP and $g_{zz} > g_{yy} > g_{xx}$, Figure 10. As additional simulations proved, and as was already shown qualitatively previously,[9] this result is stable to variations of g strain, isotropic hyperfine interaction, and iron−proton distances in reasonable limits (e.g. 0−2 MHz for the isotropic hyperfine interaction, 80−200 MHz for the line width caused by g strain and 3−3.2 Å for Fe−proton distance). The entire experimental line shapes $I(\nu_+)$, as well as the magnetic field dependence of peak intensity at $2\nu_H$, are also reproduced by simulations for $x \perp$ LP over the experimental field range (simulation indeed included all protons). The representative examples of the line

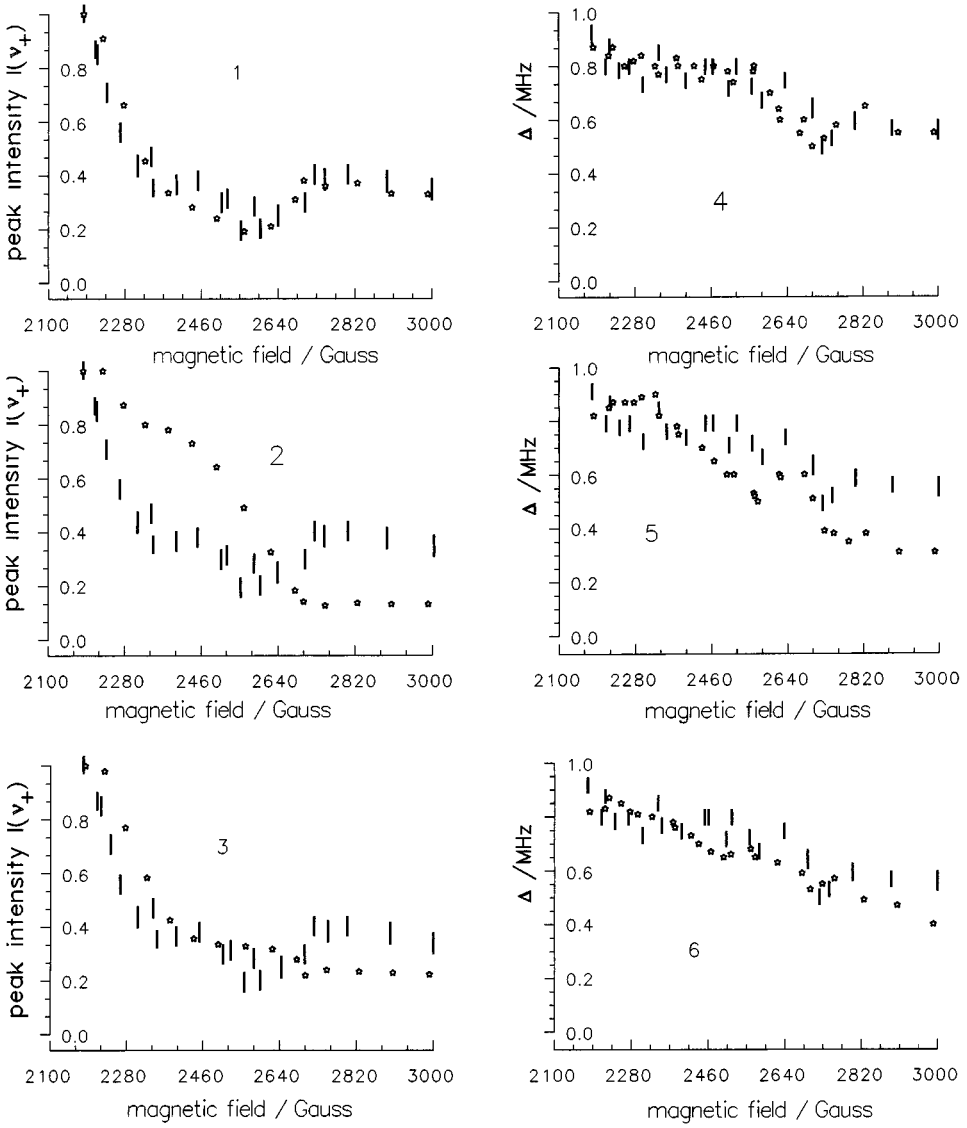

Figure 10. Experimental (bars) and calculated (stars) magnetic field strength dependences of the relative amplitudes of the NP peaks, $I(\nu_+)$, and shifts, Δ, for $[OEPFe(4\text{-}NMe_2Py)_2]^+$. The order of g values $g_{zz} > g_{yy} > g_{xx}$ was assumed, based upon the results discussed in the text. Parameters used for calculations: (1 and 4) $x \perp$ LP, (2 and 5) $x \parallel$ LP; (3 and 6) angle between x and the perpendicular to LP plane is 45°. Fe−proton distances, $r = 3.1$ Å, $r-z$ axis angle ±41°. Other details of simulation and parameters used are described in the Simulation section.

simulations are shown in Figure 7 and peak intensity with magnetic field in Figure 8. Therefore we may conclude that for this complex, the x axis of the RCF is most likely perpendicular to the LP.

To complete this part of the discussion it should be mentioned that on the basis of the numerous simulations carried out in this work, the accuracy in the mutual orientations of the LP and RCF axis may be evaluated as ≈±20°. Further increase in accuracy is possible, although it requires multifrequency experiments with continuous decrease of operational frequency, which exceeds our instrumental capabilities at the present time. Also, it must be mentioned that for both complexes the difference in the absolute amplitudes found experimentally and in simulations still exceeds the experimental error: The experimental values are less than those in the simulations by a factor 1.2−1.5. (For example, at the extreme low field position the experimental amplitude of the NP line of $[OEPFe(ImH)_2]^+$ is 16% in comparison with 22% for the simulation.) However the two-pulse spin−echo experiment always shows less absolute intensity than theory predicts, the causes of which are mainly understood yet hard to entirely overcome in experiment. The experimental difficulties include the case of partial excitation of the proton frequencies, inhomogeneity of the B_1 field in the cavity, and, as recently demonstrated in this laboratory, a finite width of the boxcar gate. All of these factors, as may be evaluated, can cause a factor of 1.3 loss in intensity which is close to that observed.

Interpretation of the g tensor Orientation Results in Terms of the Structures of the Complexes. The orientation of the **g** tensor has now been investigated in this laboratory by ESEEM spectroscopy for three model heme complexes,[9,42] and the results are helpful in understanding the relationship between the orientation of the in-plane magnetic axes g_{xx} and g_{yy} with respect to both the planar axial ligands and also the porphyrin nitrogen ligands to the metal. These results, obtained on ferriheme complexes in frozen (glassy) solutions,[9,42] confirm the existence of counter rotation of the **g** tensor with rotation of axial ligands away from the porphyrinate nitrogens: As the axial ligand rotates counterclockwise, the **g** tensor rotates clockwise about the z axis, or vice versa. This finding may help us in the future to refine the structures of such complexes in frozen solution.

(42) This work.

Of the systems we have investigated, the L = 4-(dimethylamino)pyridine case is the simplest, for the angle that describes the rotation of the projection of the ligand planes from the N_P-Fe-N_P axis, ϕ, is 41°,[24] and thus the ligands lie very close to the meso positions of the porphyrin. Because of the steric interactions between the ortho-H of the pyridine ligands and the atoms of the porphyrinate ring, this orientation, with ligands in parallel planes over two of the meso positions (structure I),[24] is expected to be the most stable, both in the solid state and in solution, in the absence of extremely bulky substituents on the porphyrinate ring. Hence, the octaethylporphyrinate complex was chosen for this study, for we could be quite sure that the distances and angles taken from the solid-state structure[24] would well reflect the structure in solution. Thus, the fact that we have determined that the smallest g value, g_{xx}, is perpendicular to the plane of the axial 4-NMe_2Py ligands, and thus lies along the direction of the filled p_π orbital of the axial ligands, is strong evidence for the counterrotation of the in-plane **g** tensor with rotation of the axial ligands away from the N_P-Fe-N_P axis. This is because we would have expected, a priori, that the p_π orbitals of the (parallel) axial ligands would determine the orientation of the d_π orbital that contains the unpaired electron and place that orbital (or rather, a linear combination of d_{xz} and d_{yz}) for maximum interaction in terms of L → Fe π donation, and hence the direction of g_{yy}, the larger of the two in-plane g values. However, with axial ligands rotated from the N_P-Fe-N_P vector by approximately 45°, we find that the magnetic axes have rotated by what appears to be 90°, so that instead of g_{yy} being along the direction of the p_π orbitals of the axial ligands, it is instead g_{xx} that lies along the p_π orbitals. This is equivalent to rotation of the **g** tensor in an equal but opposite direction with rotation of the axial ligands by ∼45°. The concept of counterrotation of the g and hyperfine tensors was first mentioned by Oosterhuis and Lang.[23] Later, single-crystal EPR studies of several model hemes[19] showed experimentally the existence of counterrotation of g_{xx} and g_{yy} with rotation of axial ligands away from the porphyrin nitrogens. We have explored the theoretical reasons for this counterrotation in the accompanying paper.[26]

For the case of L = imidazole, where ϕ = 7° in the solid state,[25] we have found that g_{xx} and g_{yy} are aligned at angles of ±45° to the p_π orbital of the imidazole ligands. Considering the structure and the findings discussed above for the case of L = 4-(dimethylamino)pyridine, we might have expected g_{yy} to be at an angle of about 14° from the p_π orbital while g_{xx} was at an angle of about 14° from the plane of the imidazoles. Or, if the degree of counterrotation is not linear with rotation of the ligands,[26] we might expect a closer coincidence of g_{xx} with the planes of the axial ligands and hence of g_{yy} with their p_π orbitals. The fact that this is not the case suggests (1) that counter-rotation may be fairly linear in this case and (2) the angle ϕ may be larger in solution than it is in the crystalline state; an angle of 22.5° would produce the exact orientation of the **g** tensor that is observed for this complex. We have recently shown by NMR techniques that the energy barrier to rotation of axial imidazoles is unmeasureably small in low-spin $[TMPCo^{III}(L)_2]^+$ complexes,[43] and, by comparison of the rotation of *hindered* ligands on $TMPCo^{III}$ and $-Fe^{III}$[43,44] it can be expected that that the energy barrier to rotation of *unhindered* imidazoles on Fe(III) is essentially zero. Hence, other factors, including solvation and hydrogen bonding of the anion of $[OEPFe(ImH)_2]^+Cl^-$ to the coordinated ligand N−H may readily dictate the orientation of the axial imidazole ligands in frozen solution, and the solution structure may therefore be somewhat different from the solid-state structure. The same is also true of the bis-pyrazole complex $[TPPFe(PzH)_2]^+Cl^-$ studied previously,[9] where the strict alignment of g_{xx} with the plane of the axial pyrazole ligands suggests that in this case, the solution structure has the pyrazole ligands lying directly over the N_P-Fe-N_P axis. However, it should be emphasized that, except for the case of g_{yy} lying along the plane of the axial ligands, as in the case of $[OEPFe(4\text{-}NMe_2\text{-}Py)_2]^+$ where the NP peak is a doublet with one peak coincident with the DP peak and hence approximately doubling its intensity, our experimental error in determining the orientation of the in-plane **g** tensor is only about ±20°. Hence, the orientations of axial ligand planes found in the crystal structures of both $[OEPFe(ImH)_2]^+$ [25] and $[TPPFe(PzH)_2]^+$ [12] and those determined by ESEEM techniques are well within these error limits, and it may be that further "refinement" of the structures is unnecessary.

Acknowledgment. The support of the National Institutes of Health, grant DK 31038 (F.A.W.), the University of Arizona Materials Characterization Program (F.A.W.), and the National Science Foundation grants DIR-9016385 for purchase of the cw EPR spectrometer and BIR-9224431 for funds to construct the pulsed EPR spectrometer is gratefully acknowledged. The authors thank Dr. Tatjana Kh. Shokhireva for preparing the samples used in this study. We are very grateful to Dr. Astashkin for providing us with source code of his filtration program.

JA9722640

(43) Polam, J. R.; Shokhireva, T. Kh.; Raffii, K.; Simonis, U.; Walker, F. A. *Inorg. Chim. Acta* **1997**, *263*, 109.

(44) Shokhirev, N. V.; Shokhireva, T. Kh.; Polam, J. R.; Watson, C. T.; Raffii, K.; Simonis, U.; Walker, F. A. *J. Phys. Chem. A* **1997**, *101*, 2778.